Inorganic & organic materials for rechargeable Li batteries with multi-electron reaction

Kai Zhang, Zhe Hu, Zhanliang Tao and Jun Chen*

Rechargeable Li batteries as electrochemical energy storage and conversion devices are continuously changing human life. In order to meet the increasing demand for energy and power density, it is essential and urgent to exploit the electrode materials with high capacity and fast charge transfer (for Li-ion and Li-S batteries) and electrocatalysts with high activity (for rechargeable Li-O_2 batteries). The high capacity is attributed to high electron transfer number and low molecular weight of the electrode materials. Combined with proper nanostructure design, the electronic transfer and ionic conductivity will be improved. This review summarizes recent efforts to apply electrode materials for Li-ion batteries with multi-electron reaction, Li-S batteries, and efficient electrocatalysts for Li-O_2 batteries. The methods to enhance the cycling and rate performance have been discussed in detail. Advanced rechargeable Li batteries with multi-electron reaction will become the research emphasis in the future.

INTRODUCTION

In modern society, electrochemical energy storage and conversion (EESC) devices have been applied in many fields such as consumer electronics, smart electricity grid, medical treatment, aerospace, and electric vehicles [1–6]. Among various EESC devices, rechargeable batteries with Li chemistry have received wide attention and undergone fast development during the last four decades because of their high operation potential and energy density, light mass, long life, high-rate capability, and environmental friendliness [7,8]. Since Li-ion batteries (LIBs) were commercialized in the early 1990s, our life has been considerably changed. However, traditional LIBs with $LiCoO_2$/graphite couple can hardly meet the increasing requirements for the life time of the devices. It is necessary and urgent to exploit novel Li-host materials with high specific energy.

The specific energy is equal to the product of electromotive force (*E*) and specific capacity (*Q*). According to thermodynamics, *E* and *Q* obey the equations as follows [5]:

$$\Delta G = -nEF, \tag{1}$$

$$Q = \frac{nF}{3.6M_w}, \tag{2}$$

where ΔG is the Gibbs free energy difference, *n* the transfer electron number, *F* the Faraday constant, M_w the molecular weight. It is very important to choose the electrode materials with high specific capacity and suitable voltage. The high specific capacity is attributed to high transfer electron number and low molecular weight.

Fig. 1 shows the discharge curves of representative cathode materials and the charge curves of representative anode materials of LIBs. For anode materials, the capacity is relatively high except for spinel $Li_4Ti_5O_{12}$ with large molecular weight. However, as to cathode materials, only
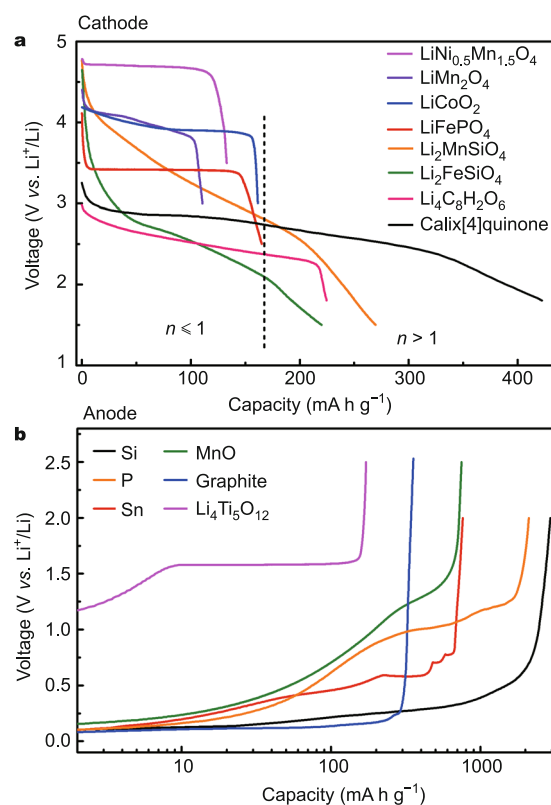

Figure 1 (a) Discharge curves of representative cathode materials and (b) charge curves of representative anode materials of LIBs.

some polyanion-type compounds and organic compounds can achieve the multi-electron reaction. Cathode materials have become a bottleneck for the development of LIBs. It is difficult to obtain a specific energy of more than 300 W h kg^{-1} for present LIBs.

Recently, Li-S and Li-O$_2$ batteries have received intense interest owing to their theoretical specific energy of more than 2500 W h kg^{-1} [9]. S and O$_2$ can react with Li via a two-electron reaction to form Li$_2$S and Li$_2$O$_2$, respectively. Nevertheless, the sluggish kinetics and poor cyclability limit their commercial step. Table 1 summarizes the electrochemical reaction, potential, transfer electron number, theoretical specific capacity, and practical capacity of the representative electrode materials of Li secondary (rechargeable) batteries. The research direction of Li secondary batteries should focus on advanced inorganic LIBs with silicate/Li$_2$S cathode and Sn/Si anode, organic LIBs with carbonyl compounds, Li-S batteries with optimal electrodes and electrolytes, and Li-O$_2$ batteries with highly active catalysts in the future.

Besides the specific energy, the specific power and cyclability are also important parameters for evaluating the electrochemical performance. To achieve the high-rate capability and long-term cyclability, methods like nanosizing (e.g., nanoparticles, nanorods, nanosheets, and nanopores),
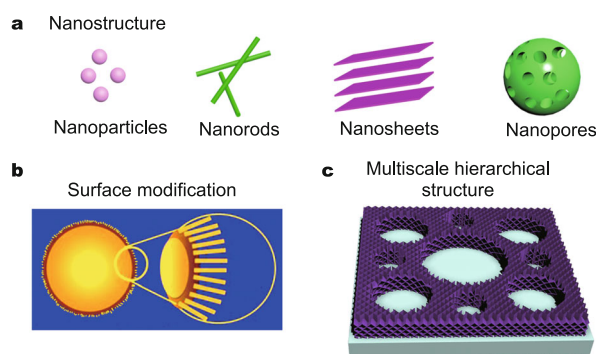

Figure 2 Schematic illustration of main strategies to improve the electrochemical performance. (a) Preparing various nanostructures (e.g., nanoparticles, nanorods, nanosheets, and nanopores), (b) surface modification, and (c) designing the multiscale hierarchical structure for electrode materials and current collectors.

surface modification, and preparing multiscale hierarchical structure are attempted (Fig. 2). Decreasing the particle size can not only enhance the utilization of active materials, but also promote the kinetics of the electrochemical reactions. In general, the diffusion time (τ) is proportional to the square of the diffusion length (L) like Equation (3) [10]:

$$\tau = \frac{L^2}{D_{Li}}. \tag{3}$$

Table 1 Electrochemical reaction, potential, transfer electron number, theoretical specific capacity, and practical capacity of the representative electrode materials of Li secondary batteries

	Electrode materials	Electrochemical reaction	Potential (V)	TEN[a]	Theoretic SC[b] (mA h g^{-1})	Practical SC (mA h g^{-1})	Ref.
Li metal batteries	FeS$_2$	FeS$_2$ + 4Li$^+$ + 4e$^-$ ↔ Fe + 2Li$_2$S	1.5	4	894	~560	[11]
	S	S + 2Li$^+$ + 2e$^-$ ↔ Li$_2$S	2.2	2	1,675	~1,100	[12]
Inorganic Li-ion batteries	Li$_3$V$_2$(PO$_4$)$_3$	Li$_3$V$_2$(PO$_4$)$_3$ ↔ V$_2$(PO$_4$)$_3$ + 3Li$^+$ + 3e$^-$	3.5/3.6/4.0	3	197	~160	[13]
	Li$_2$FeSiO$_4$	Li$_2$FeSiO$_4$ ↔ FeSiO$_4$ + 2Li$^+$ + 2e$^-$	2.8/4.8	2	332	~200	[14,15]
	Li$_2$MnSiO$_4$	Li$_2$MnSiO$_4$ ↔ MnSiO$_4$ + 2Li$^+$ + 2e$^-$	4.1/4.5	2	333	~280	[14,16]
	Li$_2$S	Li$_2$S ↔ S + 2Li$^+$ + 2e$^-$	1.7	2	1,166	~800	[17]
	Sn	Sn + 4.4Li$^+$ + 4.4e$^-$ ↔ Li$_{4.4}$Sn	0.6	4.4	990	~700	[18]
	Si	Si + 4.4Li$^+$ + 4.4e$^-$ ↔ Li$_{4.4}$Si	0.4	4.4	4,200	~3,000	[19,20]
	P	P + 3Li$^+$ + 3e$^-$ ↔ Li$_3$P	1.0	3	2,595	~2,000	[21]
	Fe$_2$O$_3$	Fe$_2$O$_3$ + 6Li$^+$ + 6e$^-$ ↔ 2Fe + 3Li$_2$O	1.5	6	1,007	~900	[22,23]
	Li$_4$Ti$_5$O$_{12}$	Li$_4$Ti$_5$O$_{12}$ + 3Li$^+$ + 3e$^-$ ↔ Li$_7$Ti$_5$O$_{12}$	1.55	3	175	~170	[24]
Organic Li-ion batteries	Li$_4$C$_8$H$_2$O$_6$(Li$_4$DHTPA)	Li$_4$C$_8$H$_2$O$_6$ ↔ Li$_2$C$_8$H$_2$O$_6$ + 2Li$^+$ + 2e$^-$	2.6	2	242	~220	[25]
		Li$_4$C$_8$H$_2$O$_6$ + 2Li$^+$ + 2e$^-$ ↔ Li$_6$C$_8$H$_2$O$_6$	0.8	2	242	~240	[25]
	C$_{16}$H$_6$O$_4$ (PTO)	C$_{16}$H$_6$O$_4$ + 4Li$^+$ + 4e$^-$ ↔ Li$_4$C$_{16}$H$_6$O$_4$	2.59	4	409	~360	[26]
	C$_{28}$H$_{16}$O$_8$(C4Q)	C$_{28}$H$_{16}$O$_8$ + 8Li$^+$ + 8e$^-$ ↔ Li$_8$C$_{28}$H$_{16}$O$_8$	2.7	8	446	~380	[27]
Li-O$_2$ batteries	O$_2$	2Li + O$_2$ ↔ Li$_2$O$_2$	2.7	2	1,675	–	[28]

a) TEN: transfer electron number; b) SC: specific capacity.

For similar Li^+ diffusion coefficient (D_{Li}), when the diffusion length is changed from 1 μm to 10 nm, the diffusion time can be reduced by four orders. Furthermore, the porous structure facilitates the accommodation of volume expansion and the infiltration of the electrolyte. Surface modification is also an effective strategy to maintain the structural stability and adjust the reaction interface. However, nanostructure is a double-edged sword, and it also suffers from the disadvantages of low tap density, undesirable side reactions, and complex synthetic method [10]. Low tap density leads to low volumetric specific capacity and specific energy, and high activity of nanomaterials may induce some side reactions such as the decomposition of the electrolyte, resulting in poor cycling performance. The synthetic method of nanomaterials is complex compared with the solid-state method, so it is difficult to meet the commercial requirements. Preparing the multiscale hierarchical structure is conducive to combine the advantages of nanomaterials and bulk materials, which improves the volumetric energy density and maintains the high performance at the same time.

In this review, recent studies about inorganic/organic electrode materials for LIBs with multi-electron reaction, Li-S batteries, and $Li-O_2$ batteries are summarized. The strategies to improve the electrochemical performance are discussed in detail. The challenges and perspectives of multi-electron reaction are also proposed.

Li-ION BATTERIES

For cathode materials of LIBs, the layered $LiCoO_2$, spinel $LiMn_2O_4$, and olivine $LiFePO_4$ allow reversible extraction/insertion of 0.5, 1 and 1 lithium per formula unit, respectively, which suffers from low capacity of less than 200 mA h g^{-1} [3]. Exploiting cathodes with high capacity is urgent. As to anodes of LIBs, most inorganic anode materials suffer from huge volume change, leading to poor cycling performance. Nanostructured anode materials can improve the electrochemical performance. Recently, organic LIBs have attracted much attention because of the high electron transfer number and low molecular weight of organic compounds. Nevertheless, the low conductivity and dissolution in organic electrolytes limit their development. In the following content, we will introduce the strategies to promote these electrode materials in detail.

Inorganic cathode materials

Among various inorganic cathode materials, polyanionic compounds such as Li_2MSiO_4 (M = Fe, Mn) and $Li_3V_2(PO_4)_3$ have attracted large attention mainly because of their high discharge capacity. The metal elements usually have viable oxidation states (e.g., $Fe^{2+}/Fe^{3+}/Fe^{4+}$, $Mn^{2+}/Mn^{3+}/Mn^{4+}$, and $V^{3+}/V^{4+}/V^{5+}$), leading to multi-electron reaction during the charge and discharge processes.

Li_2FeSiO_4

Li_2FeSiO_4 (LFSO) is environmentally friendly and cheap, and has the ability to manage two-electron reaction with a theoretical specific capacity of 332 mA h g^{-1}. As shown in Figs 3a–c, the crystal structures of LFSO are similar to Li_3PO_4 and are mainly classified into three space groups: $P2_1/n$, $Pmn2_1$, and Pmnb [14]. All the crystal structures possess tetrahedral unit like FeO_4, LiO_4, and SiO_4. In 2005, Nytén et al. [29] first reported that orthorhombic LFSO with $Pmn2_1$ space group provided one-electron reaction at 3.1 V in the first cycle. The $Pmn2_1$ phase has a β-Li_3PO_4 based structure, in which oxygen arrays form a slightly distorted hexagonal close-packed (hcp) structure and all the cations occupy half of the tetrahedral sites to form a corner-sharing network of tetrahedra (Fig. 3a). Masquelier's group [30] first prepared orthorhombic LFSO with Pmnb space group, in which the cations in the (001) plane form a succession of FeO_4/SiO_4 with opposite directions along the a axis and LiO_4 pointed in the same direction along the a axis (Fig. 3b). For monoclinic $P2_1/n$ phase (Fig. 3c), two edges are shared between FeO_4 and LiO_4, and the interlocked corner-shared FeO_4 and SiO_4 compose one-dimensional chains. The crystal structure can be controlled by adjusting the synthetic methods. Generally, the $Pmn2_1$ phase is prepared by hydrothermal method, and $P2_1/n$ and Pmnb phase are synthesized via solid state reactions at different tenperatures (600–800°C for $P2_1/n$ and ⩾900°C for Pmnb) [31–34]. Dominko's group [31] demonstrated that the stronger Fe-O bonds resulted in a lower Fe^{2+}/Fe^{3+} redox potential. The bond lengths of Fe-O in $P2_1/n$, $Pmn2_1$, and Pmnb phase are 0.2076, 0.2032, and 0.2026 nm, respectively, so Pmnb phase has the lowest redox potential. The Pmnb phase is just obtained at not lower than 900°C, and thus $P2_1/n$ phase is widely studied.

Although LFSO provides the possibility for Fe(II) to be oxidized to Fe(IV), there are still many challenges. Firstly, LFSO suffers from inferior electronic conductivity and lithium ion diffusion, which severely hinder its rate performance [35]. Secondly, the existence of site exchange for Fe and Li at the 1st cycle leads to the decrease of the operation potential [36]. Last, this electrochemical reaction is hard to achieve more than one-electron reaction at room temperature mainly because of the unstable Fe(IV) and the extremely high reaction potential (4.8 V) [35]. Therefore, intensive efforts are focused on solving the above mentioned difficulties. According to recent published papers, the effective methods include carbon modification, ion-doping, and nanocrystallization [15,32].

Carbon coating/composing is widely applied in materials with poor electronic conductivity and volume expan-

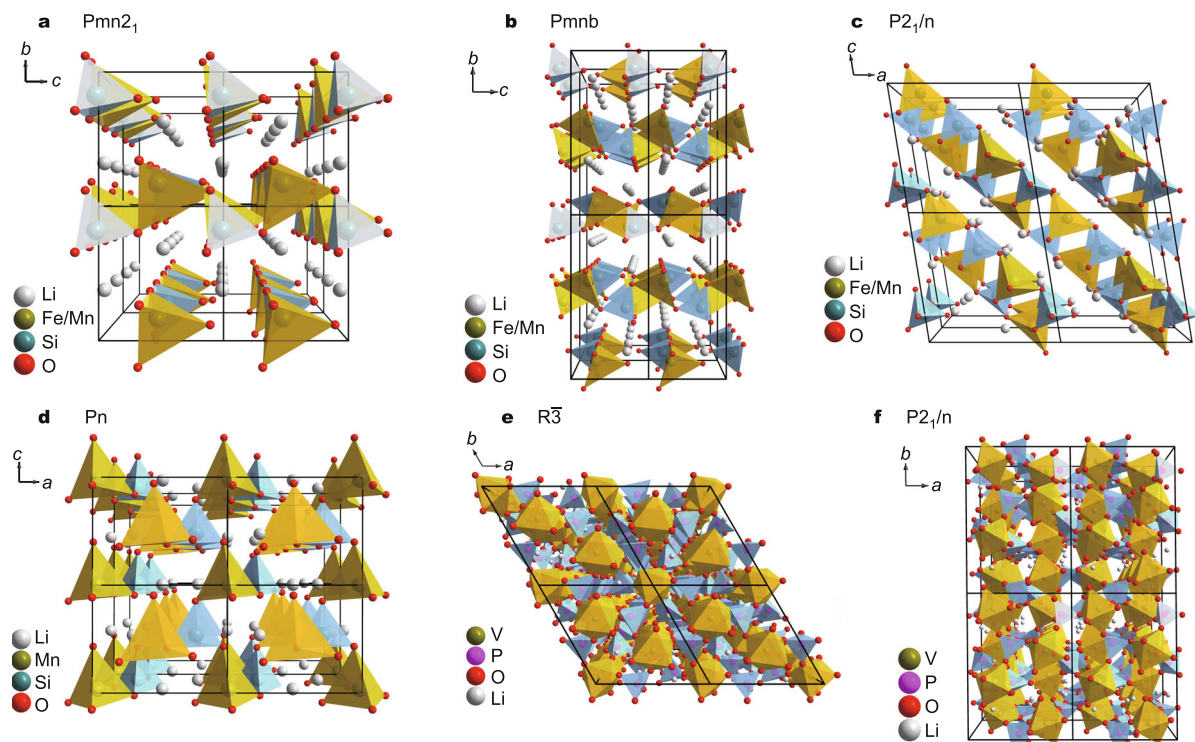**Figure 3** Crystal structures of Li_2FeSiO_4 (a–c), Li_2MnSiO_4 (a–d), and $Li_3V_2(PO_4)_3$ (e, f) polymorphs showing arrangement of FeO_4/MnO_4 tetrahedra (orange), SiO_4 tetrahedra (light blue), VO_6 octahedra (orange), and PO_4 tetrahedra (light blue) together with Li ions (white). (a) Orthorhombic $Pmn2_1$ phase; (b) orthorhombic Pmnb phase; (c) monoclinic $P2_1/n$ phase; (d) monoclinic Pn phase; (e) rhombohedral $R\bar{3}$ phase; (f) monoclinic $P2_1/n$ phase. Unit cells are indicated by black lines.

sion. Exactly for LFSO, carbon coating is the most effective way to enhance its electrochemical performance and to act as the reductant preventing the existence of Fe^{3+}. Our group synthesized spindle-like LFSO through hydrothermal synthesis [33]. Treating with *ex-situ* carbon coating, LFSO@C nanocomposites with different carbon content were obtained. Among them, the one with 7.21 wt% carbon showed high discharge capacities of 161 mA h g^{-1} at 25°C and 213 mA h g^{-1} (~1.28 e^-) at 45°C at 0.1 C. Zhu *et al.* [34] prepared macroporous graphene/LFSO through solution method by using Fe^{3+}, tetraethyl orthosilicate (TEOS), and 3D graphene as the main precursors. Because of the 3D conductive carbon network and the porous structure, the as-prepared sample displayed high capacities of 313 mA h g^{-1} at 0.1 C and 45 mA h g^{-1} at 50 C.

Nanocrystallization is another way to enhance the properties of LFSO. Although the lithium ion diffusion inside the crystal structure is rather slow, it is possible to reduce the transport time by decreasing the transport length [10]. Meanwhile, this method also provides large specific surface area contributing to more active sites for electrochemical reaction. Our group synthesized porous LFSO@C composite through tartaric-acid assisted sol-gel method. The as-prepared particles had a size of 5−20 nm [32]. The op-

timized sample showed the discharge capacities of ~180 mA h g^{-1} at 0.5 C and 102 mA h g^{-1} at 5 C. The uniformly dispersed nanoparticles with homogeneous carbon coating are the key factor for the high performance. Xia's group [37] prepared LFSO@C with a particle size of ~30 nm by a mild solvothermal method followed by thermal vapor deposition (TVD) technology. The obtained powders displayed capacities of 154 mA h g^{-1} at 1 C and 121 mA h g^{-1} at 5 C.

Because the intrinsic electronic conductivity and the lithium ion diffusion are poor, replacing partial Fe^{2+} or SiO_4^{4-} to bring some defects into the crystal structure would actually enhance the electrochemical performance. Cations like Al^{3+}, Co^{2+}, and Mn^{2+} and anions like PO_4^{3-} have proved to offer positive effect on the cell performance [14]. Qian's group [38] synthesized hierarchical mesoporous $Li_2Fe_{0.5}Mn_{0.5}SiO_4$@C and procured a high initial discharge capacity of 330 mA h g^{-1} and stable cyclic performance expressing as the remained capacity of 125 mA h g^{-1} after 60 cycles. Our group [15] synthesized $0.96Li_2FeSiO_4 \cdot 0.04LiFePO_4$@C. The doping materials showed enhanced electrochemical performance of 209 mA h g^{-1} at 15°C and 284.7 mA h g^{-1} at 45°C at 0.2 C, reduced charge transfer resistance, and improved apparent activation energy.

Li₂MnSiO₄

As another key member in the silicates family, Li₂MnSiO₄ (LMSO) also has the capability for achieving two-electron reaction (theoretical capacity of 333 mA h g⁻¹), and possesses the priorities of cheap raw materials and environmental friendliness. The already reported crystal structures of LMSO are Pmn2₁, Pmnb, P2₁/n, and Pn (Figs 3a–d) [39,40]. The first three are similar to LFSO, and monoclinic Pn phase was first reported by Abu-Lebdeh's group [40]. In Pn phase, only corner sharing takes place like Pmn2₁ phase, and MnO₄ and SiO₄ tetrahedra have the same pointing direction along the *c* axis. The relationship of crystal structure and electrochemical performance has been investigated by theoretical calculation. Arroyo-deDompablo's group [41] reported that the calculated average 2Li⁺ intercalation potentials are 4.18, 4.19, and 4.08 V for Pmnb, Pmn2₁, and P2₁/n, respectively. Fisher *et al.* [39] demonstrated that the orthorhombic Pmn2₁ phase possesses the lowest Li⁺ migration energy barrier among the four phases.

Similarly to the LFSO, LMSO also suffers from inferior electronic conductivity and lithium ion diffusion. Furthermore, LMSO has bad cyclic performance mainly due to the Jahn-Teller effect [14]. The solving methods are the same as those for LFSO: carbon modification, nanocrystallization, and ion-doping [42–44]. Yang's group [45] synthesized LMSO@C nanocomposite through solution method, and the discharge capacity was 209 mA h g⁻¹ at the 1st cycle, which was the first time to accomplish more than one-electron reaction and reversible cyclability among silicates. Our group [16] prepared core-shell structured LMSO@C nanoparticles through hydrothermal assisted solution method. The sample with carbon content of 5.15 wt% and average particle size of 22.8 nm showed the enhanced discharge capacities of 282 mA h g⁻¹ at 0.05 C and 103.4 mA h g⁻¹ at 5 C (Fig. 4). Zhang *et al.* [42] prepared Cr-doped LMSO@C nanofibers, and the nanofiber matrix provided fast electron and ion transportation leading to enhanced properties. The Li₂Mn₀.₉₄Cr₀.₀₆SiO₄@C sample possessed high discharge capacity of 318 mA h g⁻¹ at 0.05 C.

Li₃V₂(PO₄)₃

Lithium transition metal phosphate such as LiFePO₄ and LiMnPO₄ can only reach one-electron reaction, but multielectron can be altered in Li₃V₂(PO₄)₃ (LVP) during cycling. LVP exists in two main classes: rhombohedral R$\overline{3}$ phase (Fig. 3e) and monoclinic P2₁/n phase (Fig. 3f). The rhombohedral LVP possesses a two-electron reaction and displays a charge plateau at 3.8 V and a discharge plateau at 3.7 V [46]. However, rhombohedral LVP is not a thermodynamically stable phase, so most reports focus on monoclinic LVP with a high theoretical capacity of 197 mA h g⁻¹ via a three-electron reaction. The operation voltage ranges
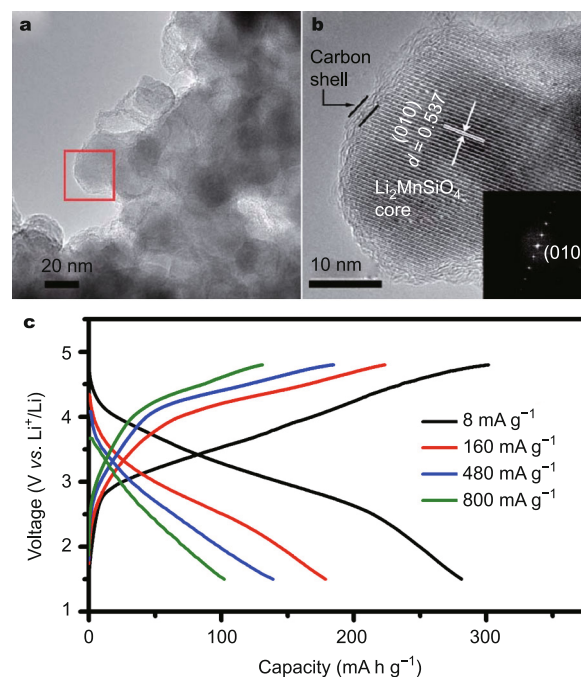

Figure 4 TEM (a) and HRTEM (b) images of LMSO@C nanoparticles. (c) Charge-discharge curves of LMSO@C at different rates. Reprinted with permission from Ref. [16]. Copyright 2013, The Royal Society of Chemistry.

from 3.0 to 4.8 V together with complex reaction processes. According to previous reports [47–49], during the charge process Li₃V₂(PO₄)₃ turns into Li₂.₅V₂(PO₄)₃ (~3.7 V) and then into Li₂V₂(PO₄)₃ (~3.8 V) with a process of V³⁺ to a mixture of V³⁺ and V⁴⁺. Keeping on Li⁺ intercalation, the Li₂V₂(PO₄)₃ transfers into LiV₂(PO₄)₃ (~4.1 V) and then V₂(PO₄)₃ (~4.6 V), with the changes of V valence from the mixture of V³⁺ and V⁴⁺ into V⁴⁺ and then the mixture of V⁴⁺ and V⁵⁺ signed on the curves. During the discharge process, the fully charged product V₂(PO₄)₃ changed to Li₂V₂(PO₄)₃ with a indistinguishable platform from 4.0 to 3.6 V as solid state behavior. Then, corresponding to the charge state, the platforms at ~3.6 and ~3.5 V represent the formation of Li₂.₅V₂(PO₄)₃ and Li₃V₂(PO₄)₃. However, a terminal charge potential at 4.8 V may lead to negative effect on the electrode material expressing as inferior cyclic performance. The modification methods for improving LVP are similar to those of LFSO. Our group [13] synthesized LVP@C nanocomposite through hydrothermal assisted sol-gel method. The uniformly dispersed particles with the size of 33 nm and homogeneously coated carbon made progress in the improved rate capabilities (~160 mA h g⁻¹ at 2 C and 120 mA h g⁻¹ at 20 C) and long-life cyclability (capacity retention of 86% after 1,000 cycles).

Other reports focus on the working voltage between 3.0 and 4.3 V, where the cell can display more stable cy-

clability without the formation of $V_2(PO_4)_3$. Li *et al.* [50] synthesized ordered macroporous LVP@C nanocomposite by using PMMA as a template. The as-prepared sample showed enhanced discharge capacities of ~156 mA h g⁻¹ at 0.1 C and 70 mA h g⁻¹ at 20 C. Zhu *et al.* [51] prepared LVP@rGO (reduced graphene oxide) nanocomposite and the procured performance showed great rate capabilities of 142 mA h g⁻¹ at 0.075 C and 119 mA h g⁻¹ at 15 C. There was no obvious decrease in the discharge capacity at 0.075 C after 50 cycles, indicating good cyclic performance.

Overall, the polyanion-type materials are suffering from the sluggish electronic conductivity and lithium ion diffusion as well as the unstable intermediates during cycling. Thus, by treating with carbon modification, nanocrystallization, or cation/anion doping, these kinds of materials would show enhanced electrochemical performance. Although there are still problems to be solved, the high theoretical capacity derived from the multi-electron reaction would have promising applications in LIBs.

Inorganic anode materials
Most inorganic anode materials have high capacities via multi-electron reaction. According to their reaction mechanism, we can divide them into three categories including alloying reaction (e.g., Sn and Si), conversion reaction (e.g., Fe_2O_3 and MnO), and intercalation reaction (e.g., $Li_4Ti_5O_{12}$).

Silicon (Si)
Si possesses a high theoretical specific capacity of 4,200 mA h g⁻¹ based on a 4.4-electron alloying reaction and a low operation voltage of ~0.4 V *vs.* Li/Li⁺ [52]. However, huge volume change of ~400% during the charge/discharge process leads to severe capacity decay and large pulverization. Furthermore, Si is a semiconductor material, and its low conductivity limits the high-rate capability. To solve those issues, two main strategies are used. One is to construct nanostructured or porous Si to relieve the strain caused by the volume change and shorten the Li⁺ ion diffusion distance [19,20,53,54]. Our group [20] prepared nest-like Si nanospheres by solvothermal method, and the Si nanospheres delivered discharge capacities of 3,628 mA h g⁻¹ at 0.4 A g⁻¹ and 3,052 mA h g⁻¹ at 2 A g⁻¹. Cui's group [19] designed and synthesized double-walled silicon nanotubes with high charge capacities of 2,971 mA h g⁻¹ at 2 A g⁻¹ and 940 mA h g⁻¹ at 12 C as well as capacity retention of 88% after 6,000 cycles. Meanwhile, introducing other elements or polymers can buffer the volume change and improve the conductivity [55–57]. Wang and coworkers [57] synthesized Si/C fiber paper by electrospraying, and the Si/C composite showed a reversible capacity of ~1,200 mA h g⁻¹ after 100 cycles at 0.5 A g⁻¹. Our group [58,59] used mag-

netron sputtering to prepare Si-Y and sandwich-like Ti/Si/Ti thin film anode. The metallic buffer layer suppressed the volume variation of Si and enhanced the Li⁺ ion diffusion kinetics. Chen and coworkers [56] fabricated polypyrrole (PPY)@porous hollow Si spheres which showed the outstanding cycling stability with capacity retention of 88% after 250 cycles at 1 A g⁻¹ compared with the second capacity.

Tin (Sn)
Sn has also attracted intensive interest owing to its high theoretical specific capacity of 990 mA h g⁻¹ based on a 4.4-electron alloying reaction. Nevertheless, Sn is also plagued by large volume change. To maintain the structural stability, many Sn-based composites have been attempted [18,60–65]. Our group prepared ultrasmall Sn nanoparticles with a particle size of ~5 nm homogenously embedded in N-doped porous carbon (5-Sn/C) by carbonizing the Sn (Salen) (Fig. 5) [18]. The Sn/C composite showed an initial discharge capacity of 1,014 mA h g⁻¹ with capacity retention of 71.2% after 200 cycles at 0.2 A g⁻¹. Even at a high current density of 5 A g⁻¹, a reversible capacity of ~480 mA h g⁻¹ was obtained. Our group also reported the synthesis of the pitaya-like Sn@C nanocomposite via an aerosol spray pyrolysis route [65]. In the composite, Sn nanoparticles with a particle size of ~8 nm are uniformly dispersed in the carbon spheres. The composite delivered a capacity of 410 mA h g⁻¹ after 1,000 cycles at 4,000 mA g⁻¹
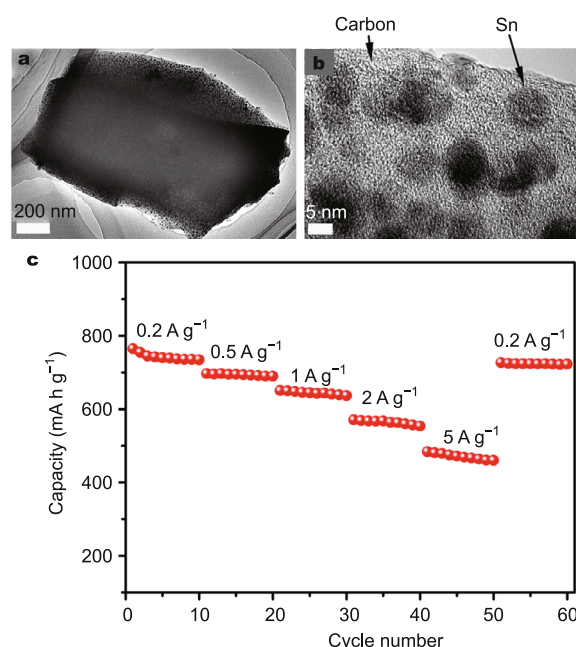

Figure 5 (a) TEM image, (b) HRTEM image, and (c) rate capability of ultrasmall Sn nanoparticles dispersed in N-doped porous carbon matrix (5-Sn/C). Reprinted with permission from Ref. [18]. Copyright 2013, American Chemical Society.

(6.1 C). Cho's group [63] synthesized core-shell Sn-Cu nanoalloys with a particle size of 10 nm, and the Sn-Cu composite displayed a charge capacity of 620 mA h g^{-1} at 6 C.

Phosphorus (P)

P is another promising anode material with a theoretical specific capacity of 2,595 mA h g^{-1} based on the reaction of $3Li + P \leftrightarrow Li_3P$. However, P suffers from dramatic capacity fade after a few cycles because of its large volume expansion and poor conductivity. So far, there are only a few reports about P, in which P-C composites have been used to overcome the problems [21,66,67]. He's group [21] prepared P-C composite by heating the mixture of red P and porous carbon at 450°C in a seal vessel. The composite exhibited an initial capacity of 2,413 mA h g^{-1} with capacity retention of 87% from the 2nd to 55th cycle at 100 mA g^{-1}, but the P content is only 30.56 wt%. Sohn and co-authors [67] reported a carbon/black P composite with an initial discharge capacity of 2,010 mA h g^{-1}. Nevertheless, black P is a thermodynamically unstable phase, which is very difficult to synthesize. P anode still faces the problems how to increase the content of P and improve the electrochemical performance.

Metal oxides

Metal oxides can react with Li$^+$ through a conversion reaction as follows [68]:

$$M_xO_y + 2yLi^+ + 2ye^- \leftrightarrow xM + yLi_2O \qquad (4)$$

$$(M: Fe, Co, Ni, Mn, etc.).$$
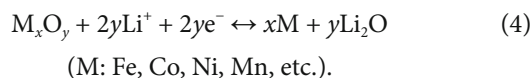
Though metal oxides possess high theoretical specific capacity, they suffer from severe structural change resulted from conversion reactions, which makes it difficult for them to achieve long-term cyclability. Designing the nanostructure/porous structure and preparing M_xO_y/C composite are effective means to keep the structural stability. Our group used templating method to synthesize α-Fe$_2$O$_3$ and Co$_3$O$_4$ nanotubes with high initial capacities, but the cycling performance was not ideal [22,69]. Cho's group [23] produced spindle-like porous α-Fe$_2$O$_3$ by using metal organic framework (MOF) as a template. The porous α-Fe$_2$O$_3$ showed a reversible capacity of 911 mA h g^{-1} after 50 cycles at 0.2 C. Even at a high rate of 10 C, the discharge capacity still reached 424 mA h g^{-1}. Sun *et al.* [70] fabricated MnO/graphene composite which presented reversible capacities of 2,014.1 mA h g^{-1} at 0.2 A g^{-1} and 843.3 mA h g^{-1} at 2 A g^{-1}. The specific capacity exceeded the theoretical value, because Mn(II) was further oxidized to Mn(IV) which contributed to supernumerary capacity. Although many efforts have been made to improve the performance of the metal oxides with conversion reactions, their commercialization is still difficult to achieve because of their relatively high operation potential and severe structural damage.

Li$_4$Ti$_5$O$_{12}$

Spinel Li$_4$Ti$_5$O$_{12}$ (LTO) can react with 3Li$^+$ to form Li$_7$Ti$_5$O$_{12}$, and its potential plateau is ~1.55 V which avoids the formation of lithium dendrites. In addition, the structure of LTO does not change during the charge/discharge process, leading to outstanding cyclability. However, the intrinsically low electrical conductivity and Li ion diffusion coefficient of LTO limit its rate performance. To overcome these issues, two methods are proposed. One is to reduce the particle size or design the nanoporous structure [71–73]. Feckl *et al.* [72] prepared highly porous LTO with a surface area of 205 m^2 g^{-1} and a uniform pore size of 7 nm by hydrothermal method combined with heating treatment. The porous LTO delivered ultrahigh-rate capabilities (173 mA h g^{-1} at 100 C and 128 mA h g^{-1} at 800 C). Lou's group [73] reported a simple templating method for the synthesis of mesoporous LTO hollow spheres, exhibiting a reversible capacity of ~120 mA h g^{-1} after 300 cycles at 5 C. The other is surface coating with carbon materials or oxides [24,74–76]. Our group investigated the effect of the coated carbon of LTO on its electrochemical performance by *in situ* Raman spectroscopy [24]. Through balancing the electronic conduction and the ionic transport, the carbon content could be optimized. Guo's and Wan's group [75] reported rutile-TiO$_2$ coated LTO nanosheets with a discharge capacity of 149 mA h g^{-1} after 100 cycles at 20 C. The TiO$_2$ layer enhanced the surface stability and cycle life. Although LTO only has a theoretical specific capacity of 175 mA h g^{-1}, it has exhibited high-rate capability and long life, so it can be applied for the EESC devices with high specific power.

Although anode materials have large specific capacity except for LTO, they usually suffer from large volume change during Li$^+$ intercalation and deintercalation. Nanostructured Sn/C and Si/C composites deliver improved cycling and rate performance, which offers a great promise for next-generation LIBs.

Organic carbonyl compounds

Organic electrode materials, especially organic carbonyl compounds, possess high capacity because of their high transfer electron number and low molecular weight. The electrochemical redox reactions of organic carbonyl compounds are two- or multi-electron transfer processes. For example, benzoquinone (BQ) first gains one electron to generate radical anion (BQ$^{•-}$), and then gains another electron to form BQ^{2-} (Fig. 6).

Up to now, there have been some interesting results for organic electrode materials. Fig. 7 shows the molecular structure and theoretical specific capacity of the repre-
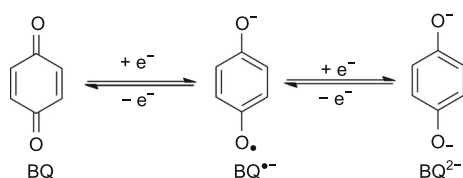
Figure 6 Electrochemical redox reaction mechanism of benzoquinone (BQ).

BQ
(2e, 496 mA h g^{-1})

AQ
(2e, 257 mA h g^{-1})

PID
(2e, 255 mA h g^{-1})

BDTD
(2e, 244 mA h g^{-1})

BFFD
(2e, 285 mA h g^{-1})

PQ
(2e, 257 mA h g^{-1})

PhenQ
(2e, 255 mA h g^{-1})

BDTQ
(2e, 244 mA h g^{-1})

PTO
(4e, 409 mA h g^{-1})

PHP
(2e, 182 mA h g^{-1})

NTCDA
(2e, 200 mA h g^{-1})

NTCDM
(2e, 182 mA h g^{-1})

C4Q
(4e, 446 mA h g^{-1})

BNQ
(4e, 341 mA h g^{-1})

H$_2$HNQ
(4e, 310 mA h g^{-1})

Li$_2$C$_6$H$_2$O$_4$
(2e, 353 mA h g^{-1})

Li$_2$C$_6$O$_6$
(4e, 589 mA h g^{-1})

Li$_4$C$_6$O$_6$
(2e, 274 mA h g^{-1})

Li$_2$C$_8$H$_4$O$_4$
(2e, 301 mA h g^{-1})
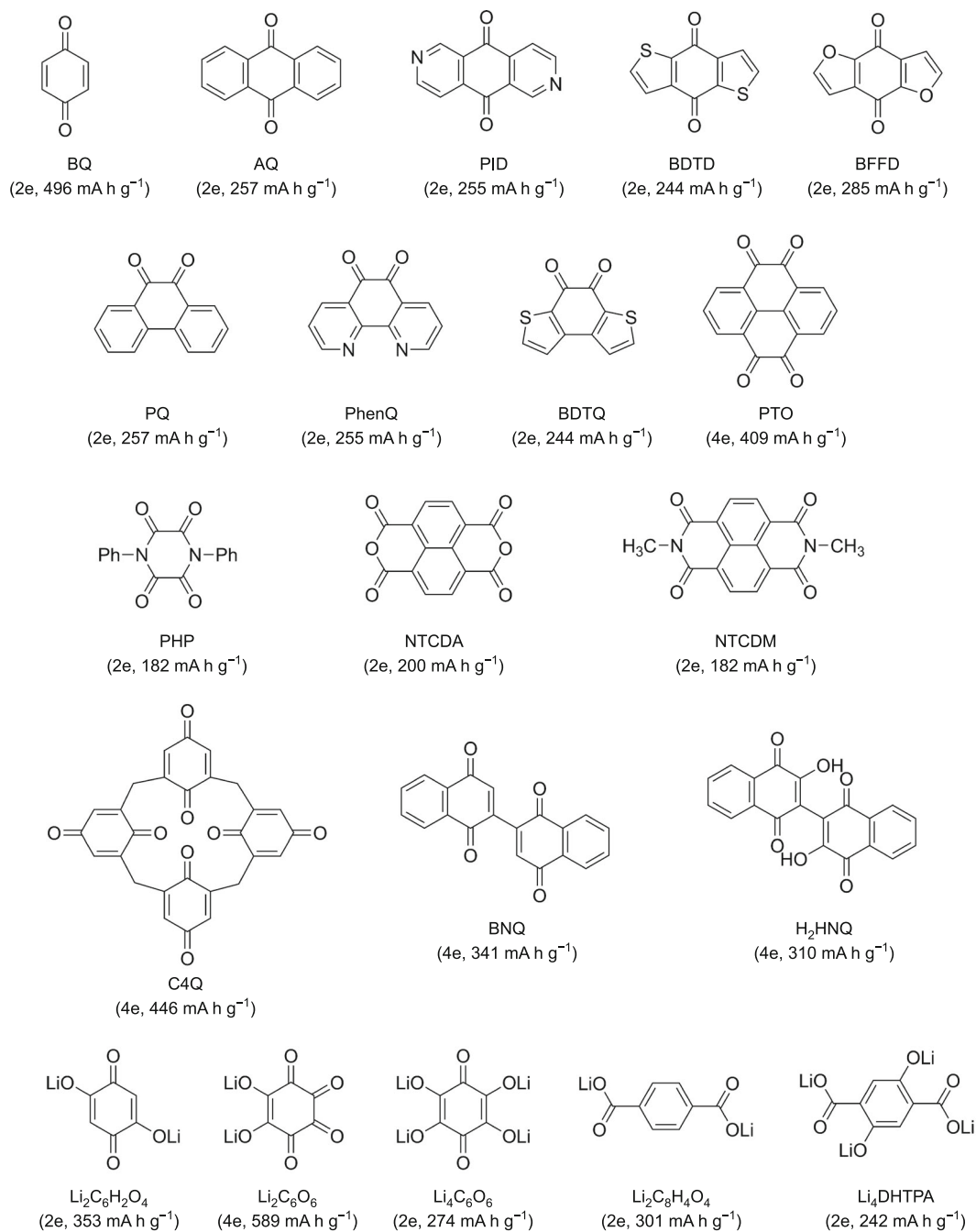
Li$_4$DHTPA
(2e, 242 mA h g^{-1})

Figure 7 Molecular structure and theoretical specific capacity of the representative organic carbonyl compounds.

sentative organic carbonyl compounds. Although organic carbonyl compounds are greatly various, they receive less concern than inorganic electrode materials for a long time, because of their intrinsically low electrical conductivity and easy dissolution in organic electrolytes like Li-S batteries. Recently, much progress has been made, such as molecular-level engineering design, increasing the molecular weight by polymerization, enhancing the polarity by using organic lithium salts, and enveloping the active materials in a conductive container [77,78].

Molecular engineering design
Though organic compounds are easy to design and processing, there are only a few reports on the molecular-level engineering design of organic electrode materials. Our group used the density functional theory (DFT) calculations to predict the average discharge voltage and the active site availability of organic carbonyl compounds [26,79]. The linear relationship between the discharge potential and the calculated lowest unoccupied molecular orbital (LUMO) energy of fused heteroaromatic organic compounds was first proposed. Low LUMO energy is favorable to improve the discharge potential. According to our calculated results, a series of fused heteroaromatic organic compounds were designed and prepared, including furan (benzofuro[5,6-b]furan-4,8-dione, BFFD), thiophene (benzo[1,2-b:4,5-b']dithiophene-4,8-dione, BDTD), and pyridine (pyrido[3,4-g]isoquinoline-5,10-dione, PID) [79]. These compounds as cathode materials of LIBs presented higher operation potential, cyclability, and rate performance than those of benzene-fused analogue (anthraquinone, AQ). Especially, BFFD showed a discharge capacity of 181 mA h g^{-1} at a high rate of 100 C. We also first proposed to use the highest occupied molecular orbital plots and thermodynamic energy change of organic carbonyl compounds to predict carbonyl utilization, which explained that for organic compounds with four carbonyl groups, why four-electron reaction could occur in pyrene-4,5,9,10-tetraone (PTO) and dilithium rhodizonate salt (Li$_2$C$_6$O$_6$), while only two-electron reaction could occur in N,N'-diphenyl-2,3,5,6-tetraketopiperazine (PHP) and 1,4,5,8-naphthalenetetracarboxylic dianhydride (NTCDA) [26].

Restriction of dissolution
Increasing the molecular weight by polymerization and enhancing the polarity by using organic lithium salts both can reduce the dissolution of organic electrode materials, leading to improved cycling performance. Nokami *et al.* [80] prepared polymer-bound PTO (PPYT) which delivered an initial discharge capacity of 231 mA h g^{-1} and capacity retention of 83% after 500 cycles at 1 C. Tarascon's group [81,82] synthesized lithium salts of tetrahydroxybenzo-

quinone and terephthalic acid (Li$_2$C$_6$O$_6$ and Li$_2$C$_8$H$_4$O$_4$). Li$_2$C$_6$O$_6$ showed a reversible capacity of ~200 mA h g^{-1} at 2.7 V via a two-electron reaction to form Li$_2$C$_6$O$_6$, and lithium-salted Li$_2$C$_8$H$_4$O$_4$ exhibited a stable capacity of 234 mA h g^{-1} after 50 cycles with a potential plateau of 0.8 V. Combining the two molecules, our group developed tetra-lithium salts of 2,5-dihydroxyterephthalic acid (Li$_4$C$_8$H$_2$O$_6$) nanosheets as both cathode and anode materials [25]. For cathode, a two-electron reaction could occur with the redox couple Li$_4$C$_8$H$_2$O$_6$/Li$_2$C$_8$H$_2$O$_6$ at ~2.6 V, and for anode, a two-electron reaction could occur with the redox couple Li$_4$C$_8$H$_2$O$_6$/Li$_6$C$_8$H$_2$O$_6$ at ~0.8 V. The all-organic LIBs delivered a reversible capacity of 225 mA h g^{-1} with an average operation voltage of ~1.8 V.

Besides optimizing the organic molecules, the quasi-solid-state electrolytes can also improve the cycling performance. Our group demonstrated that a poly(methacrylate) (PMA)/poly(ethylene glycol) (PEG) based gel polymer electrolyte (GPE) could be used as the electrolyte of organic LIBs with high capacity [27,83]. The PMA/PEG-based GPE combined with calix[4]quinone (C4Q) and pillar[5] quinone (P5Q) to form two quasi-solid-state LIBs. The quasi-solid-state LIBs with C4Q delivered an initial discharge capacity of 422 mA h g^{-1} at 0.2 C and a reversible capacity of 379 mA h g^{-1} after 100 cycles [27], and P5Q displayed an initial capacity of 410 mA h g^{-1} with capacity retention of 88.5% after 100 cycles [83].

Improvement of conductivity
Carbon materials have high electronic conductivity, which is favorable to improve the Li$^+$ diffusion kinetics of organic carbonyl compounds, leading to high rate performance. Moreover, some porous carbon materials can confine the organic small molecule to reduce its dissolution in organic electrolytes. Our group developed a facile ultrasonic method to prepare 2,2'-bis(3-hydroxy-1,4-naphthoquinone) (H$_2$BHNQ)/mesoporous CMK-3 carbon composite with 50 wt% H$_2$BHNQ [84]. The composite showed discharge capacities of 308.6 mA h g^{-1} at 0.1 C and 124.0 mA h g^{-1} at 10 C. Song *et al.* [85] synthesized poly(anthraquinonyl sulfide) (PAQS)-graphene nanocomposite which showed a discharge capacity of 100 mA h g^{-1} at a high rate of 100 C.

Although organic carbonyl compounds have developed rapidly in the past few years, their operation potential is difficult to exceed 3.0 V. Exploiting the organic carbonyl compounds with high operation potential and practical capacity is urgent and necessary in the future.

Li-S BATTERIES
Li–S batteries with a two-electron reaction possess a high specific capacity of 1,675 mA h g^{-1} and a high specific energy of 2,600 W h kg^{-1}. The sulfur cathode usually discharges

with two plateaus at ~2.3 V and ~1.95 V, corresponding to the redox couples of S_8/Li_2S_x ($x = 4-8$) and Li_2S_x ($x = 4-8$)/Li_2S, respectively. Although the concept of Li-S batteries was proposed in the 1940s, they have developed rapidly only after 2009 [86]. Two main factors limit the electrochemical performance of Li-S batteries [9]. One is low conductivity and large volume change of sulfur, leading to sluggish kinetics and poor cyclability. The other is that the intermediate long-chain lithium polysulfides are very soluble in organic electrolytes, which causes the "shuttle loss". Because carbonate-based electrolytes react with polysulfides [87], we have to use expensive ether-based electrolytes, leading to high cost of Li-S batteries. Of course, safety issue derived from Li dendrite is a problem of all Li metal batteries. To solve these problems, many strategies have been proposed, including preparing the carbon-sulfur composite, optimizing the organic electrolytes, and using the short-chain S_{2-4} and Li_2S alternative to S_8 [88,89].

Carbon-sulfur composite and conducting polymer coating
Encapsulating sulfur in carbon materials and/or conducting polymers is a most commonly used means to improve the conductivity and constrain the "shuttle loss". Nazar's group [86] prepared polyethylene glycol (PEG)-coated CMK-3/S composite, and the composite delivered a capacity of 1,320 mA h g^{-1} at 0.1 C. CMK-3 as conductive mesoporous carbon framework accommodates the volume change during the charge-discharge process, improves the adsorption capability, and enhances the Li$^+$ diffusion kinetics. Polymer modification further inhibits the dissolution of lithium ploysulfides and provides a chemical diffusion gradient.

Besides mesoporous carbon, other carbon materials such as graphene, carbon nanotubes, carbon fibers, and porous carbon spheres are also attempted [90–93]. Our group [12] reported a composite of sulfur impregnated in porous hollow carbon spheres (PHCS) with high discharge capacities of 1,450 mA h g^{-1} at 0.05 C and 1,068 mA h g^{-1} at 0.5 C (Fig. 8). The high performance is attributed to the high electronic conductivity and hierarchical porous structure of PHCS. Wang's group [93] synthesized 3D hyperbranched hollow carbon nanorods (CNR) as a sulfur container, and the CNR/S nanocomposite displayed specific capacities of 1,378 mA h g^{-1} at 0.1 C and 663 mA h g^{-1} at 10 C.

Conducting polymers such as poly(3,4-ethylenedioxythio phene) (PEDOT), polypyrrole (PPY), polyaniline (PANI), and polyacrylonitrile (PAN) have been explored to envelop the sulfur [94–98]. The polymer coating can not only physically confine the dissolution of lithium polysulfides, but also chemically bond with lithium polysulfides. Cui's group [96] prepared three polymer/hollow sulfur nanosphere composites, and their performance decreased in the order of PEDOT > PPY > PANI because of their dif-
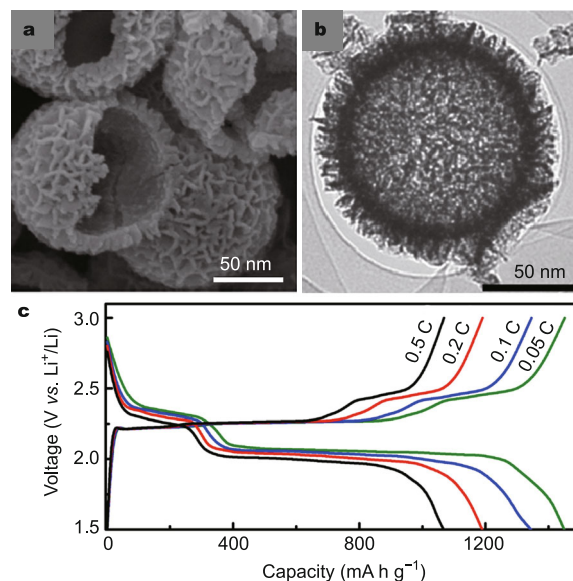

Figure 8 SEM (a) and TEM (b) images of porous hollow carbon sphere (PHCS)/S nanocomposite. (c) Charge and discharge curves of PHCS/S nanocomposite at different rates. Reprinted with permission from Ref. [12]. Copyright 2013, Tsinghua University Press and Springer-Verlag.

ferent conductivities. It was found that S–PAN composite showed a reversible capacity of ~800 mA h g^{-1} and high capacity retention of more than 98.1% after 50 cycles at 100 mA g^{-1} [97].

Small sulfur molecules
In most reports, stable cyclooctasulfur (cyclo-S_8) is used as the cathode of Li-S batteries. Involuntarily, when melt sulfur is impregnated into the microporous carbon, metastable small sulfur molecules (S_{2-4}) are found [99]. The small sulfur molecules discharge with only one plateau at ~1.9 V, which avoids the formation of long-chain lithium polysulfides and essentially solves the "shuttle loss". Furthermore, carbonate-based electrolytes can be used in this Li-S battery system, which substantially lower the cost. Guo's and Wan's group [99] first reported small sulfur molecules embedded in a microporous carbon with a pore size of ~0.5 nm, and the composite showed an initial capacity of 1,670 mA h g^{-1} at 0.1 C and a reversible capacity of 1,142 mA h g^{-1} after 200 cycles. However, it is difficult to achieve high sulfur content for the microporous carbon, so combining the advantages of mesoporous carbon and microporous carbon is necessary. Li et al. [100] prepared ordered meso-microporous core-shell carbon (MMCS)/S composite which exhibited a capacity of 837 mA h g^{-1} at 0.5 C after 200 cycles. The mesoporous carbon "core" possesses large pore volume to improve the load amount of sulfur, and the microporous carbon "shell" has a strong adsorbing ability to inhibit the dissolution of polysulfides.

Li$_2$S cathode

To solve the safety hazard of Li dendrite, Cui's group [101] proposed to use Li$_2$S cathode coupled with lithium-free high-capacity anodes (e.g., Si and Sn) to compose a novel Li-ion battery. Li$_2$S has a theoretical specific capacity of 1,166 mA h g^{-1}, and the breakage of its volume contraction is less than volume expansion of sulfur electrode during the first charge process. However, Li$_2$S also suffers from low electronic conductivity and "shuttle loss". The efforts used in the sulfur cathode are attempted to solve the problems of Li$_2$S cathode. Manthiram's group [102] fabricated a sandwiched electrode with bulky Li$_2$S powder in the middle and self-weaving carbon nanotubes on both sides. At 0.1 C, a discharge capacity of 838 mA h g^{-1} was obtained. Cui's group [103] prepared PPY/Li$_2$S composites via *in-situ* polymerization method. The N atoms of PPY could form Li–N bond with Li$_2$S, which confined the dissolution of polysulfides. The PPY/Li$_2$S composites exhibited a discharge capacity of 785 mA h g^{-1} with excellent cycling stability at 0.2 C. Li's group [104] synthesized the core-shell structured Li$_2$S@C spheres with particle size of 1 μm via a chemical vapor deposition (CVD) method. The Li$_2$S@C spheres showed stable cycling performance, and when the Li$_2$S content reached 88 wt% in the electrode, the morphology of the electrode still changed little after 400 cycles at 0.5 C.

In addition, Li$_2$S is plagued by the large potential barrier during the first charge process, leading to a utilized capacity penalty. Although setting a high charging cutoff voltage (more than 4 V) can compulsively activate Li$_2$S, it results in unnecessary energy loss. Downsizing Li$_2$S particles combined with a highly conductive matrix can boost the electrode kinetics, which benefits the activation of Li$_2$S [105]. Our group [17] prepared ultrafine Li$_2$S nanoparticles (~8.5 nm) uniformly dispersed in graphene nanosheets. The graphene/Li$_2$S nanocomposite presented an initial discharge capacity of 1,119 mA h g^{-1} and almost invisible potential barrier in the first cycle at 0.02 C. At a high rate of 2 C, the discharge capacity still reached 565 mA h g^{-1}. The graphene/Li$_2$S nanocomposite also combined with the Si thin film anode to form a full cell, and the full cell exhibited a high discharge capacity of 900 mA h g^{-1} at 0.05 C. The Li$_2$S/Si full cell offers promising application toward the development of high-energy LIBs.

Electrolyte

Electrolyte is also very important to cycling performance of Li-S batteries. For cyclo-S$_8$, the polysulfides can chemically react with the carbonate-based electrolytes, so ether-based electrolytes are usually used. Furthermore, LiNO$_3$ can form a passive film on the surface of lithium metal to prevent the reaction between polysulfides and Li, so LiNO$_3$

are usually used as an electrolyte additive to improve the Coulombic efficiency [106,107]. Hu's group [108] designed a new "solvent-in-salt" (SIS) electrolyte with 7 M salt concentration. The SIS electrolyte inhibited the dissolution of lithium polysulfides, avoided the formation of lithium dendrites, and led to capacity retention of 74% after 100 cycles at 0.2 C.

Though the electrochemical performance of Li-S batteries is continuously improved, the sulfur content still needs to be increased. If the practical specific energy, volumetric energy density, and cycling performance are further enhanced, the Li-S batteries would bring a breakthrough to EESC devices.
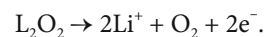
Li-O$_2$ BATTERIES

Recently, rechargeable Li-O$_2$ batteries have received a great deal of interest because of their high theoretical specific energy of 5,200 W h kg^{-1}, which is 10 times larger than that of traditional LIBs with LiCoO$_2$/graphite couple [109,110]. Bruce and coworkers [111,112] proposed the reaction mechanism of Li-O$_2$ batteries in nonaqueous electrolytes as follows:

oxygen reduction reaction (ORR):

$$O_2 + e^- \rightarrow O_2^-,$$

$$O_2^- + Li^+ \rightarrow LiO_2,$$

$$2LiO_2 \rightarrow L_2O_2 + O_2;$$
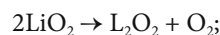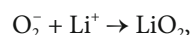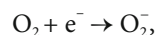
oxygen evolution reaction (OER):

$$L_2O_2 \rightarrow 2Li^+ + O_2 + 2e^-.$$

The theoretical potential of Li-O$_2$ batteries is 2.96 V, but the practical discharge and charge potentials are ~2.7 and over 4.0 V, respectively. The large overpotential is attributed to sluggish kinetics of ORR/OER. In addition, the discharge product (i.e., Li$_2$O$_2$) has poor conductivity and insolubility, which may completely cover the catalyst to prevent further reaction and increase the electrical resistance of air cathode, leading to low capacity and poor rate and cycling performance. To overcome the above problems, designing suitable cathode with large specific surface area, highly active catalysts, and porous nanostructure is very important.

The ORR/OER catalysts can be divided into three categories: carbon materials [113], noble metals or alloys [114–118], and metal oxides [119–127]. Table 2 lists the electrochemical performance of some representative catalysts for Li-O$_2$ batteries. Kang's group [113] used hierarchically aligned porous carbon nanotube (CNT) fibril as the air electrode, which delivered a capacity of 1,700 mA h g^{-1} at a high current density of 5,000 mA g^{-1}. Peng *et al.* [115] developed a porous gold electrode with high capacity retention of 95% after 100 cycles at 500 mA g^{-1}. Zhang and coworkers [119] prepared porous La$_{0.75}$Sr$_{0.25}$MnO$_3$ nano-

Table 2 Discharge capacity, cycling performance, and rate capability of Li-O_2 batteries with the representative catalysts

Catalysts	Maximum capacity based on total mass	Cycling performance/ cutoff capacity	Rate capability	Ref.
3D hierarchically aligned porous CNT fibril	~3,000 mA h g^{-1} at 2,000 mA g^{-1}	80 cycles/1,000 mA h g^{-1}	1,700 mA h g^{-1} at 5,000 mA g^{-1}	[113]
Porous Au electrode	~320 mA h g^{-1} at 500 mA g^{-1}	capacity retention of 95% after 100 cycles	–	[115]
Ru@multi-walled carbon nanotube paper	22,600 mA h g^{-1} at 500 mA g^{-1}	50 cycles/5,000 mA h g^{-1}	–	[116]
Pd-modified hollow spherical carbon/carbon paper	12,254 mA h g^{-1} at 500 mA g^{-1}	205 cycles/1,000 mA h g^{-1}	1,900 mA h g^{-1} at 800 mA g^{-1}	[118]
Sponge-like ε-MnO_2 on Ni foam	7,000 mA h g^{-1} at 100 mA g^{-1}	100 cycles/1,000 mA h g^{-1}	1,900 mA h g^{-1} at 800 mA g^{-1}	[132]
Hierarchical porous ε-MnO_2 on Ni foam	5,700 mA h g^{-1} at 100 mA g^{-1}	190 cycles/800 mA h g^{-1}	~3,400 mA h g^{-1} at 800 mA g^{-1}	[28]
Spinel $MnCo_2O_4$/graphene hybrid	3,784 mA h g^{-1} at 100 mA g^{-1}	40 cycles/1,000 mA h g^{-1}	2,743 mA h g^{-1} at 800 mA g^{-1}	[120]
Porous perovskite $CaMnO_3$ nanostructure	~3,670 mA h g^{-1} at 35 mA g^{-1}	80 cycles/500 mA h g_{carbon}^{-1}	~1,830 mA h g^{-1} at 105 mA g^{-1}	[134]
Porous perovskite $La_{0.75}Sr_{0.25}MnO_3$ nanotubes	~11,000 mA h g^{-1} at 16.7 mA g^{-1}	124 cycles/1,000 mA h g^{-1}	~3,890 mA h g^{-1} at 133 mA g^{-1}	[119]

tubes (PNT-LSM) as an ORR/OER catalyst. The air electrode with PNT-LSM could be cycled over 124 cycles while the capacity was limited at 1,000 mA h g^{-1}. These reports demonstrated that 3D porous nanostructure is conducive to the electron and O_2 transport, Li^+ diffusion, and restriction of Li_2O_2 growth, leading to excellent cycling and rate performance.

To decrease the charge potential, some soluble catalysts such as tetrathiafulvalene (TTF), LiI, and iron phthalocyanine (FePc) are proposed [128–131]. Compared with solid catalysts, the soluble catalysts are more advantageous to catalyze the decomposition of Li_2O_2. Bruce's group [128] demonstrated that the TTF molecule was oxidized to form TTF^+, and then TTF^+ reacted with the solid Li_2O_2 to be reduced back to TTF. The charge plateau could maintain at 3.5 V during 100 cycles at 1 mA cm^{-2}. Wu's group [131] reported the use of an I_3^-/I^- redox couple to combine the photoelectrode of dye-sensitized solar cells with the oxygenelectrode Li-O_2 batteries. Through utilizing solar energy, the charge plateau decreased to 3.4 V at 0.032 mA cm^{-2}. Sun *et al.* [129] found that FePc could serve as not only a ORR/OER catalyst but also a shuttle of $(O_2)^-$ species and electrons between the surface of the conductive carbon and the insulator Li_2O_2.

Among various ORR/OER catalysts, Mn-based oxides have attracted much interest because of their low cost, high abundance, environmental friendliness, and high catalytic activity. Our group synthesized a series of nanostructured Mn-based oxides such as hierarchical porous ε-MnO_2, spinel Co-Mn-O nanoparticles, and porous perovskite $CaMnO_3$-Pt nanocomposite [28,121,132–135]. As shown in Fig. 9, hierarchical porous ε-MnO_2 on Ni foam was prepared by a facile electrodeposition method using oxygen as a bubble

template [28]. The composite delivered discharge capacities of 5,700 mA h g^{-1} at 100 mA g^{-1} and ~3,400 mA h g^{-1} at 800 mA g^{-1}. When limiting the capacity to 800 mA h g^{-1}, the terminal discharge voltage could exceed 2.2 V for 190 cycles at 500 mA g^{-1}. We also investigated the size effect of Li_2O_2 on charge potential, and the small particle size facilitated the decrease of charge overpotential [136].

Besides catalysts, the electrolytes and anodes are also very important for the electrochemical performance of Li-O_2 batteries [112], but only a few reports focus on this aspect. Furthermore, the experimental capacity of Li-O_2 batteries is calculated based on the mass of catalysts. This method makes it very difficult to compare different systems, and the real specific energy and energy density are also difficult to determine. How to find a reasonable evaluation method is what we should discuss in the future.

CONCLUSIONS AND OUTLOOK

A series of electrode materials have been applied for LIBs with multi-electron reaction and Li-S batteries, and various catalysts have been attempted to promote the two-electron reaction of Li-O_2 batteries. The strategies to improve practical capacity, cycling and rate performance have also been widely studied. Generally, Li rechargeable batteries with multi-electron reaction can obtain a capacity of more than 200 mA h g^{-1} for the active material. Furthermore, nanostructured materials facilitate both electronic transport and ionic diffusion, leading to high rate performance. Thus, combining nanomaterials with multi-electron reaction is the research direction in the future.

For cathodes of LIBs, silicate-type Li_2MnSiO_4 possesses a high theoretical specific capacity of ~333 mA h g^{-1} via a two-electron reaction, but it is plagued by low conduc-
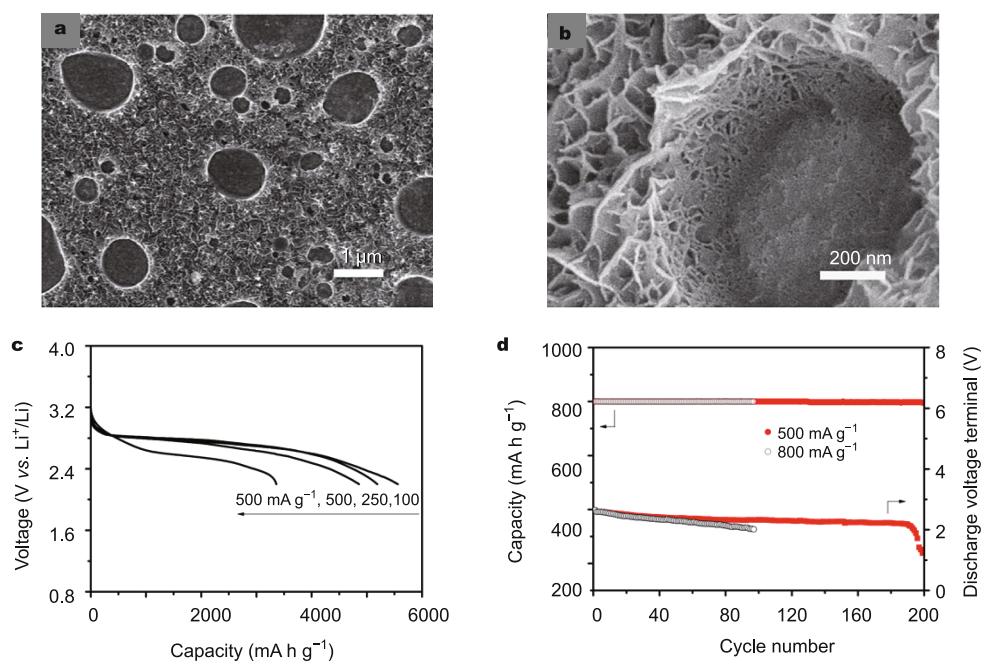
Figure 9 (a, b) SEM images of hierarchical porous ε-MnO$_2$ at different scales; (c) rate performance of hierarchical porous ε-MnO$_2$; (d) variation of terminal discharge voltage on cycling at current densities of 500 and 800 mA g^{-1}. Reprinted with permission from Ref. [28]. Copyright 2014, Wiley-VCH.

tivity and poor structural stability. Although the surface coating and downsizing the particle size partially relieve the problems, it cannot absolutely solve its low intrinsic conductivity. Doping other cations or anions may enhance the structural stability and Li$^+$ diffusion kinetics. Core-shell structured Li$_2$MnSiO$_4$@C nanocomposites have delivered great improvements on the rate and cycling performance. However, only a few reports focus on increasing the operation potential of Li$_2$MnSiO$_4$ by cation doping such as Co and Ni. As to anodes of LIBs, most inorganic anode materials can achieve multi-electron reaction to obtain high capacity, but their volume change is huge, leading to poor cycling performance. Nanostructured anode materials with surface modification have improved the electrochemical performance, which offers a great promise for next-generation LIBs with high energy. Recently, organic LIBs have attracted a lot of attention because of high electron transfer number and low molecular weight of organic electrode materials. Nevertheless, the low conductivity and easy dissolution in organic electrolytes limit their development. Using lithium salts of organic carbonyl compounds combined with highly conductive carbon materials are promising in the applications of green organic LIBs.

For Li-S batteries, C/S nanocomposite and ether-based electrolytes have been widely used as cathodes and electrolytes. However, low sulfur content in the electrodes decreases thire practical specific energy, and expensive ether-based electrolytes increase the cost. If nano S is di-

rectly loaded on the 3D porous current collector (e.g., carbon paper), the specific energy would be improved greatly. Small sulfur molecules with carbonate-based electrolytes and Li$_2$S coupled with Si or Sn anode are also promising research directions.

For Li-O$_2$ batteries, extensive fundamental studies focus on using highly active catalysts to improve the sluggish kinetics. Mn-based oxides along with various 3D porous nanostructures are particularly attractive. Compared with the discharge mechanism, the charge process is more difficult to understand, so more *in-situ* characterizations should be used to observe the charge process. In addition, learning from nature may help us to find more suitable structures to achieve highly effective and fast ORR/OER since biology embodies such characteristics.

Improving the operation potential of multi-electron reaction and volumetric energy density of Li rechargeable batteries should be the focus of future studies. Great opportunities and challenges still coexist in electrode materials with multi-electron reaction.

1   Dunn B, Kamath H, Tarascon JM. Electrical energy storage for the grid: a battery of choices. Science, 2011, 334: 928–935
2   Goodenough JB. Evolution of strategies for modern rechargeable batteries. Acc Chem Res, 2012, 46: 1053–1061
3   Cheng F, Liang J, Tao Z, Chen J. Functional materials for recharge-

able batteries. Adv Mater, 2011, 23: 1695–1715

4 Chen J, Cheng F. Combination of lightweight elements and nanostructured materials for batteries. Acc Chem Res, 2009, 42: 713–723

5 Zhang K, Han X, Hu Z, *et al.* Nanostructured Mn-based oxides for electrochemical energy storage and conversion. Chem Soc Rev, doi: 10.1039/C4CS00218K

6 Tao Z, Chen J. Secondary battery systems for energy storage in smart grids. Chin Sci Bull, 2012, 57: 2545–2560

7 Song HK, Lee KT, Kim MG, Nazar LF, Cho J. Recent progress in nanostructured cathode materials for lithium secondary batteries. Adv Funct Mater, 2010, 20: 3818–3834

8 Zhou Z, Tian N, Li J, Broadwell I, Sun S. Nanomaterials of high surface energy with exceptional properties in catalysis and energy storage. Chem Soc Rev, 2011, 40: 4167–4185

9 Bruce PG, Freunberger SA, Hardwick LJ, Tarascon JM. Li-O_2 and Li-S batteries with high energy storage. Nat Mater, 2012, 11: 19–29

10 Wang Y, Li H, He P, Hosono E, Zhou H. Nano active materials for lithium-ion batteries. Nanoscale, 2010, 2: 1294–1305

11 Liu J, Wen Y, Wang Y, *et al.* Carbon-encapsulated pyrite as stable and earth-abundant high energy cathode material for rechargeable lithium batteries. Adv Mater, 2014, 26: 6025–6030

12 Zhang K, Zhao Q, Tao Z, Chen J. Composite of sulfur impregnated in porous hollow carbon spheres as the cathode of Li-S batteries with high performance. Nano Res, 2013, 6: 38–46

13 Duan W, Hu Z, Zhang K, *et al.* $Li_3V_2(PO_4)_3$@C core-shell nanocomposite as a superior cathode material for lithium-ion batteries. Nanoscale, 2013, 5: 6485–6490

14 Gong Z, Yang Y. Recent advances in the research of polyanion-type cathode materials for Li-ion batteries. Energy Environ Sci, 2011, 4: 3223–3242

15 Gao H, Hu Z, Zhang K, Cheng F, Chen J. Intergrown Li_2FeSiO_4·$LiFePO_4$-C nanocomposites as high-capacity cathode materials for lithium-ion batteries. Chem Commun, 2013, 49: 3040–3042

16 Hu Z, Zhang K, Gao H, *et al.* Li_2MnSiO_4@C nanocomposite as a high-capacity cathode material for Li-ion batteries. J Mater Chem A, 2013, 1: 12650–12656

17 Zhang K, Wang L, Hu Z, Cheng F, Chen J. Ultrasmall Li_2S nanoparticles anchored in graphene nanosheets for high-energy lithium-ion batteries. Sci Rep, 2014, 4: 6467

18 Zhu Z, Wang S, Du J, *et al.* Ultrasmall Sn nanoparticles embedded in nitrogen-doped porous carbon as high-performance anode for lithium-ion batteries. Nano Lett, 2013, 14: 153–157

19 Wu H, Chan G, Choi JW, *et al.* Stable cycling of double-walled silicon nanotube battery anodes through solid-electrolyte interphase control. Nat Nanotech, 2012, 7: 310–315

20 Ma H, Cheng F, Chen J, *et al.* Nest-like silicon nanospheres for high-capacity lithium storage. Adv Mater, 2007, 19: 4067–4070

21 Wang L, He X, Li J, *et al.* Nano-structured phosphorus composite as high-capacity anode materials for lithium batteries. Angew Chem Int Ed, 2012, 51: 9034–9037

22 Chen J, Xu L, Li W, Gou X. α-Fe_2O_3 nanotubes in gas sensor and lithium-ion battery applications. Adv Mater, 2005, 17: 582–586

23 Xu X, Cao R, Jeong S, Cho J. Spindle-like mesoporous α-Fe_2O_3 anode material prepared from MOF template for high-rate lithium batteries. Nano Lett, 2012, 12: 4988–4991

24 Zhu Z, Cheng F, Chen J. Investigation of effects of carbon coating on the electrochemical performance of $Li_4Ti_5O_{12}$/C nanocomposites. J Mater Chem A, 2013, 1: 9484–9490

25 Wang S, Wang L, Zhang K, *et al.* Organic $Li_4C_8H_2O_6$ nanosheets for lithium-ion batteries. Nano Lett, 2013, 13: 4404–4409

26 Liang Y, Zhang P, Chen J. Function-oriented design of conjugated carbonyl compound electrodes for high energy lithium batteries. Chem Sci, 2013, 4: 1330–1337

27 Huang W, Zhu Z, Wang L, *et al.* Quasi-solid-state rechargeable lithium-ion batteries with a calix[4]quinone cathode and gel polymer

electrolyte. Angew Chem Int Ed, 2013, 52: 9162–9166

28 Hu X, Cheng F, Han X, Zhang T, Chen J. Oxygen bubble-templated hierarchical porous ε-MnO_2 as a superior catalyst for rechargeable Li-O_2 batteries. Small, doi: 10.1002/smll.201401790

29 Nytén A, Abouimrane A, Armand M, Gustafsson T, Thomas JO. Electrochemical performance of Li_2FeSiO_4 as a new Li-battery cathode material. Electrochem Commun, 2005, 7: 156–160

30 Boulineau A, Sirisopanaporn C, Dominko R, *et al.* Polymorphism and structural defects in Li_2FeSiO_4. Dalton Trans, 2010, 39: 6310–6316

31 Sirisopanaporn C, Masquelier C, Bruce PG, Armstrong AR, Dominko R. Dependence of Li_2FeSiO_4 electrochemistry on structure. J Am Chem Soc, 2010, 133: 1263–1265

32 Zheng Z, Wang Y, Zhang A, *et al.* Porous Li_2FeSiO_4/C nanocomposite as the cathode material of lithium-ion batteries. J Power Sources, 2012, 198: 229–235

33 Gao H, Hu Z, Zhang K, *et al.* Hydrothermal synthesis of spindle-like Li_2FeSiO_4-C composite as cathode materials for lithium-ion batteries. J Energy Chem, 2014, 23: 274–281

34 Zhu H, Wu X, Zan L, Zhang Y. Three-dimensional macroporous graphene-Li_2FeSiO_4 composite as cathode material for lithium-ion batteries with superior electrochemical performances. ACS Appl Mater Interfaces, 2014, 6: 11724–11733

35 Gao H, Hu Z, Yang J, Chen J. $Li_{2-x}Fe_{1-x}Al_xSiO_4$/C nanocomposites cathodes for lithium-ion batteries. Energy Technol, 2014, 2: 355–361

36 Nyten A, Kamali S, Haggstrom L, Gustafsson T, Thomas JO. The lithium extraction/insertion mechanism in Li_2FeSiO_4. J Mater Chem, 2006, 16: 2266–2272

37 Yi J, Hou M, Bao H, *et al.* In-situ generation of Li_2FeSiO_4/C nanocomposite as cathode material for lithium ion battery. Electrochim Acta, 2014, 133: 564–569

38 Jiang X, Xu H, Liu J, *et al.* Hierarchical mesoporous $Li_2Mn_{0.5}Fe_{0.5}SiO_4$ and $Li_2Mn_{0.5}Fe_{0.5}SiO_4$/C assembled by nanoparticles or nanoplates as a cathode material for lithium-ion batteries. Nano Energy, 2014, 7: 1–9

39 Fisher CAJ, Kuganathan N, Islam MS. Defect chemistry and lithium-ion migration in polymorphs of the cathode material Li_2MnSiO_4. J Mater Chem A, 2013, 1: 4207–4214

40 Duncan H, Kondamreddy A, Mercier PHJ, *et al.* Novel Pn polymorph for Li_2MnSiO_4 and its electrochemical activity as a cathode material in Li-ion batteries. Chem Mater, 2011, 23: 5446–5456

41 Arroyo-deDompablo ME, Dominko R, Gallardo-Amores JM, *et al.* On the energetic stability and electrochemistry of Li_2MnSiO_4 polymorphs. Chem Mater, 2008, 20: 5574–5584

42 Zhang S, Lin Z, Ji L, *et al.* Cr-doped Li_2MnSiO_4/carbon composite nanofibers as high-energy cathodes for Li-ion batteries. J Mater Chem, 2012, 22: 14661–14666

43 Liu J, Xu H, Jiang X, Yang J, Qian Y. Facile solid-state synthesis of Li_2MnSiO_4/C nanocomposite as a superior cathode with a long cycle life. J Power Sources, 2013, 231: 39–43

44 He G, Manthiram A. Nanostructured Li_2MnSiO_4/C cathodes with hierarchical macro-/mesoporosity for lithium-ion batteries. Adv Funct Mater, 2014, 24: 5277–5283

45 Li Y, Gong Z, Yang Y. Synthesis and characterization of Li_2MnSiO_4/C nanocomposite cathode material for lithium ion batteries. J Power Sources, 2007, 174: 528–532

46 Gaubicher J, Wurm C, Goward G, Masquelier C, Nazar L. Rhombohedral form of $Li_3V_2(PO_4)_3$ as a cathode in Li-ion batteries. Chem Mater, 2000, 12: 3240–3242

47 Huang H, Yin SC, Kerr T, Taylor N, Nazar LF. Nanostructured composites: a high capacity, fast rate $Li_3V_2(PO_4)_3$/carbon cathode for rechargeable lithium batteries. Adv Mater, 2002, 14: 1525–1528

48 Yin SC, Grondey H, Strobel P, Huang H, Nazar LF. Charge ordering in lithium vanadium phosphates: electrode materials for lithi-

um-ion batteries. J Am Chem Soc, 2003, 125: 326–327

49 Yin SC, Grondey H, Strobel P, Anne M, Nazar LF. Electrochemical property: structure relationships in monoclinic $Li_{3-y}V_2(PO_4)_3$. J Am Chem Soc, 2003, 125: 10402–10411

50 Li D, Tian M, Xie R, et al. Three-dimensionally ordered macroporous $Li_3V_2(PO_4)_3$/C nanocomposite cathode material for high-capacity and high-rate Li-ion batteries. Nanoscale, 2014, 6: 3302–3308

51 Zhu X, Yan Z, Wu W, et al. Manipulating size of $Li_3V_2(PO_4)_3$ with reduced graphene oxide: towards high-performance composite cathode for lithium ion batteries. Sci Rep, 2014, 4: 5768

52 Wu H, Cui Y. Designing nanostructured Si anodes for high energy lithium ion batteries. Nano Today, 2012, 7: 414–429

53 Ge M, Lu Y, Ercius P, et al. Large-scale fabrication, 3D tomography, and lithium-ion battery application of porous silicon. Nano Lett, 2013, 14: 261–268

54 Kim H, Han B, Choo J, Cho J. Three-dimensional porous silicon particles for use in high-performance lithium secondary batteries. Angew Chem Int Ed, 2008, 47: 10151–10154

55 Ng SH, Wang J, Wexler D, et al. Highly reversible lithium storage in spheroidal carbon-coated silicon nanocomposites as anodes for lithium-ion batteries. Angew Chem Int Ed, 2006, 45: 6896–6899

56 Du F, Li B, Fu W, et al. Surface binding of polypyrrole on porous silicon hollow nanospheres for Li-ion battery anodes with high structure stability. Adv Mater, 2014, 26: 6145–6150

57 Xu Y, Zhu Y, Han F, Luo C, Wang C. 3D Si/C fiber paper electrodes fabricated using a combined electrospray/electrospinning technique for Li-ion batteries. Adv Energy Mater, doi: 10.1002/aenm. 201400753

58 Li H, Bai H, Tao Z, Chen J. Si-Y multi-layer thin films as anode materials of high-capacity lithium-ion batteries. J Power Sources, 2012, 217: 102–107

59 Guo S, Li H, Bai H, Tao Z, Chen J. Ti/Si/Ti sandwich-like thin film as the anode of lithium-ion batteries. J Power Sources, 2014, 248: 1141–1148

60 Hassoun J, Derrien G, Panero S, Scrosati B. A nanostructured Sn-C composite lithium battery electrode with unique stability and high electrochemical performance. Adv Mater, 2008, 20: 3169–3175

61 Zhang W, Hu J, Guo Y, et al. Tin-nanoparticles encapsulated in elastic hollow carbon spheres for high-performance anode material in lithium-ion batteries. Adv Mater, 2008, 20: 1160–1165

62 Xu Y, Liu Q, Zhu Y, et al. Uniform nano-Sn/C composite anodes for lithium ion batteries. Nano Lett, 2013, 13: 470–474

63 Kim MG, Sim S, Cho J. Novel core-shell Sn-Cu anodes for lithium rechargeable batteries prepared by a redox-transmetalation reaction. Adv Mater, 2010, 22: 5154–5158

64 Ke F, Huang L, Jamison L, et al. Nanoscale tin-based intermetallic electrodes encapsulated in microporous copper substrate as the negative electrode with a high rate capacity and a long cycleability for lithium-ion batteries. Nano Energy, 2013, 2: 595–603

65 Zhang N, Zhao Q, Han X, Yang J, Chen J. Pitaya-like Sn@C nanocomposites as high-rate and long-life anode for lithium-ion batteries. Nanoscale, 2014, 6: 2827–2832

66 Qian J, Qiao D, Ai X, Cao Y, Yang H. Reversible 3-Li storage reactions of amorphous phosphorus as high capacity and cycling-stable anodes for Li-ion batteries. Chem Commun, 2012, 48: 8931–8933

67 Park CM, Sohn HJ. Black phosphorus and its composite for lithium rechargeable batteries. Adv Mater, 2007, 19: 2465–2468

68 Cabana J, Monconduit L, Larcher D, Palacín MR. Beyond intercalation-based Li-ion batteries: the state of the art and challenges of electrode materials reacting through conversion reactions. Adv Mater, 2010, 22: E170–E192

69 Li WY, Xu LN, Chen J. Co_3O_4 nanomaterials in lithium-ion batteries and gas sensors. Adv Funct Mater, 2005, 15: 851–857

70 Sun Y, Hu X, Luo W, Xia F, Huang Y. Reconstruction of conformal nanoscale MnO on graphene as a high-capacity and long-life anode material for lithium ion batteries. Adv Funct Mater, 2013, 23: 2436–2444

71 Chen S, Xin Y, Zhou Y, et al. Self-supported $Li_4Ti_5O_{12}$ nanosheet arrays for lithium ion batteries with excellent rate capability and ultralong cycle life. Energy Environ Sci, 2014, 7: 1924–1930

72 Feckl JM, Fominykh K, Döblinger M, Fattakhova-Rohlfing D, Bein T. Nanoscale porous framework of lithium titanate for ultrafast lithium insertion. Angew Chem Int Ed, 2012, 51: 7459–7463

73 Yu L, Wu HB, Lou XW. Mesoporous $Li_4Ti_5O_{12}$ hollow spheres with enhanced lithium storage capability. Adv Mater, 2013, 25: 2296–2300

74 Zhao L, Hu Y, Li H, Wang Z, Chen L. Porous $Li_4Ti_5O_{12}$ coated with N-doped carbon from ionic liquids for Li-ion batteries. Adv Mater, 2011, 23: 1385–1388

75 Wang Y, Gu L, Guo Y, et al. Rutile-TiO_2 nanocoating for a high-rate $Li_4Ti_5O_{12}$ anode of a lithium-ion battery. J Am Chem Soc, 2012, 134: 7874–7879

76 Liu J, Song K, van Aken PA, Maier J, Yu Y. Self-supported $Li_4Ti_5O_{12}$–C nanotube arrays as high-rate and long-life anode materials for flexible Li-ion batteries. Nano Lett, 2014, 14: 2597–2603

77 Liang Y, Tao Z, Chen J. Organic electrode materials for rechargeable lithium batteries. Adv Energy Mater, 2012, 2: 742–769

78 Wang S, Tao Z, Chen J. Organic conjugated carbonyl compounds as electrode materials for lithium-ion batteries. Chin Sci Bull, 2013, 58: 3132–3139

79 Liang Y, Zhang P, Yang S, Tao Z, Chen J. Fused heteroaromatic organic compounds for high-power electrodes of rechargeable lithium batteries. Adv Energy Mater, 2013, 3: 600–605

80 Nokami T, Matsuo T, Inatomi Y, et al. Polymer-bound pyrene-4, 5,9,10-tetraone for fast-charge and -discharge lithium-ion batteries with high capacity. J Am Chem Soc, 2012, 134: 19694–19700

81 Chen H, Armand M, Courty M, et al. Lithium salt of tetrahydroxybenzoquinone: toward the development of a sustainable Li-ion battery. J Am Chem Soc, 2009, 131: 8984–8988

82 Armand M, Grugeon S, Vezin H, et al. Conjugated dicarboxylate anodes for Li-ion batteries. Nat Mater, 2009, 8: 120–125

83 Zhu Z, Guo D, Tao Z, Chen J. Pillar[5]quinone as cathode material for quasi-solid-state rechargeable lithium batteries. Sci Sin Chim, 2014, 44: 1175–1180

84 Li H, Duan W, Zhao Q, et al. 2,2'-Bis(3-hydroxy-1,4-naphthoquinone)/CMK-3 nanocomposite as cathode material for lithium-ion batteries. Inorg Chem Front, 2014, 1: 193–199

85 Song Z, Xu T, Gordin ML, et al. Polymer-graphene nanocomposites as ultrafast-charge and -discharge cathodes for rechargeable lithium batteries. Nano Lett, 2012, 12: 2205–2211

86 Ji X, Lee KT, Nazar LF. A highly ordered nanostructured carbon-sulphur cathode for lithium-sulphur batteries. Nat Mater, 2009, 8: 500–506

87 Gao J, Lowe MA, Kiya Y, Abruña HD. Effects of liquid electrolytes on the charge-discharge performance of rechargeable lithium/sulfur batteries: electrochemical and in-situ X-ray absorption spectroscopic studies. J Phys Chem C, 2011, 115: 25132–25137

88 Yang Y, Zheng G, Cui Y. Nanostructured sulfur cathodes. Chem Soc Rev, 2013, 42: 3018–3032

89 Yin Y, Xin S, Guo Y, Wan L. Lithium-sulfur batteries: electrochemistry, materials, and prospects. Angew Chem Int Ed, 2013, 52: 13186–13200

90 Jayaprakash N, Shen J, Moganty SS, Corona A, Archer LA. Porous hollow carbon@sulfur composites for high-power lithium-sulfur batteries. Angew Chem Int Ed, 2011, 50: 5904–5908

91 Yang X, Zhang L, Zhang F, Huang Y, Chen Y. Sulfur-infiltrated graphene-based layered porous carbon cathodes for high-performance lithium-sulfur batteries. ACS Nano, 2014, 8: 5208–5215

92 Elazari R, Salitra G, Garsuch A, Panchenko A, Aurbach D. Sulfur-impregnated activated carbon fiber cloth as a binder-free cathode for rechargeable Li-S batteries. Adv Mater, 2011, 23: 5641–5644

93   Chen S, Huang X, Liu H, *et al.* 3D hyperbranched hollow carbon nanorod architectures for high-performance lithium-sulfur batteries. Adv Energy Mater, doi: 10.1002/aenm.201301761

94   Yang Y, Yu G, Cha JJ, *et al.* Improving the performance of lithium-sulfur batteries by conductive polymer coating. ACS Nano, 2011, 5: 9187–9193

95   Fu Y, Manthiram A. Enhanced cyclability of lithium-sulfur batteries by a polymer acid-doped polypyrrole mixed ionic-electronic conductor. Chem Mater, 2012, 24: 3081–3087

96   Li W, Zhang Q, Zheng G, *et al.* Understanding the role of different conductive polymers in improving the nanostructured sulfur cathode performance. Nano Lett, 2013, 13: 5534–5540

97   Wang L, He X, Li J, *et al.* Analysis of the synthesis process of sulphur-poly(acrylonitrile)-based cathode materials for lithium batteries. J Mater Chem, 2012, 22: 22077–22081

98   Yin L, Wang J, Lin F, Yang J, Nuli Y. Polyacrylonitrile/graphene composite as a precursor to a sulfur-based cathode material for high-rate rechargeable Li-S batteries. Energy Environ Sci, 2012, 5: 6966–6972

99   Xin S, Gu L, Zhao N, *et al.* Smaller sulfur molecules promise better lithium-sulfur batteries. J Am Chem Soc, 2012, 134: 18510–18513

100   Li Z, Jiang Y, Yuan L, *et al.* A highly ordered meso@microporous carbon-supported sulfur@smaller sulfur core-shell structured cathode for Li-S batteries. ACS Nano, 2014, 8: 9295–9303

101   Yang Y, McDowell MT, Jackson A, *et al.* New nanostructured Li_2S/silicon rechargeable battery with high specific energy. Nano Lett, 2010, 10: 1486–1491

102   Fu Y, Su Y-S, Manthiram A. Li_2S-carbon sandwiched electrodes with superior performance for lithium-sulfur batteries. Adv Energy Mater, doi: 10.1002/aenm.201300655

103   Seh ZW, Wang H, Hsu PC, *et al.* Facile synthesis of Li_2S-polypyrrole composite structures for high-performance Li_2S cathodes. Energy Environ Sci, 2014, 7: 672–676

104   Nan C, Lin Z, Liao H, *et al.* Durable carbon-coated Li_2S core-shell spheres for high performance lithium/sulfur cells. J Am Chem Soc, 2014, 136: 4659–4663

105   Cai K, Song MK, Cairns EJ, Zhang Y. Nanostructured Li_2S–C composites as cathode material for high-energy lithium/sulfur batteries. Nano Lett, 2012, 12: 6474–6479

106   Yang Y, Zheng G, Misra S, *et al.* High-capacity micrometer-sized Li_2S particles as cathode materials for advanced rechargeable lithium-ion batteries. J Am Chem Soc, 2012, 134: 15387–15394

107   Aurbach D, Pollak E, Elazari R, *et al.* On the surface chemical aspects of very high energy density, rechargeable Li–sulfur batteries. J Electrochem Soc, 2009, 156: A694–A702

108   Suo L, Hu Y, Li H, Armand M, Chen L. A new class of Solvent-in-Salt electrolyte for high-energy rechargeable metallic lithium batteries. Nat Commun, 2013, 4: 1481

109   Wang Z, Xu D, Xu J, Zhang X. Oxygen electrocatalysts in metal-air batteries: from aqueous to nonaqueous electrolytes. Chem Soc Rev, 2014, 43: 7746–7786

110   Cheng F, Chen J. Nanoporous catalysts for rechargeable Li-air batteries. Acta Chim Sin, 2013, 71: 473–477

111   Peng Z, Freunberger SA, Hardwick LJ, *et al.* Oxygen reactions in a non-aqueous Li^+ electrolyte. Angew Chem Int Ed, 2011, 50: 6351–6355

112   Cheng F, Chen J. Metal-air batteries: from oxygen reduction electrochemistry to cathode catalysts. Chem Soc Rev, 2012, 41: 2172–2192

113   Lim HD, Park KY, Song H, *et al.* Enhanced power and rechargeability of a Li–O_2 battery based on a hierarchical-fibril CNT electrode. Adv Mater, 2013, 25: 1348–1352

114   Lu Y, Gasteiger HA, Shao-Horn Y. Catalytic activity trends of oxygen reduction reaction for nonaqueous Li-air batteries. J Am Chem Soc, 2011, 133: 19048–19051

115   Peng Z, Freunberger SA, Chen Y, Bruce PG. A reversible and higher-rate Li-O_2 battery. Science, 2012, 337: 563–566

116   Li F, Chen Y, Tang DM, *et al.* Performance-improved Li-O_2 battery with Ru nanoparticles supported on binder-free multi-walled carbon nanotube paper as cathode. Energy Environ Sci, 2014, 7: 1648–1652

117   Du J, Cheng F, Wang S, Zhang T, Chen J. M(Salen)-derived nitrogen-doped M/C (M = Fe, Co, Ni) porous nanocomposites for electrocatalytic oxygen reduction. Sci Rep, 2014, 4: 4386

118   Xu J, Wang Z, Xu D, Zhang L, Zhang X. Tailoring deposition and morphology of discharge products towards high-rate and long-life lithium-oxygen batteries. Nat Commun, 2013, 4: 2438

119   Xu J, Xu D, Wang Z, *et al.* Synthesis of perovskite-based porous $La_{0.75}Sr_{0.25}MnO_3$ nanotubes as a highly efficient electrocatalyst for rechargeable lithium-oxygen batteries. Angew Chem Int Ed, 2013, 52: 3887–3890

120   Wang H, Yang Y, Liang Y, *et al.* Rechargeable Li-O_2 batteries with a covalently coupled $MnCo_2O_4$-graphene hybrid as an oxygen cathode catalyst. Energy Environ Sci, 2012, 5: 7931–7935

121   Cheng F, Shen J, Peng B, *et al.* Rapid room-temperature synthesis of nanocrystalline spinels as oxygen reduction and evolution electrocatalysts. Nat Chem, 2011, 3: 79–84

122   Cheng F, Zhang T, Zhang Y, *et al.* Enhancing electrocatalytic oxygen reduction on MnO_2 with vacancies. Angew Chem Int Ed, 2013, 52: 2474–2477

123   Han X, Zhang T, Du J, Cheng F, Chen J. Porous calcium-manganese oxide microspheres for electrocatalytic oxygen reduction with high activity. Chem Sci, 2013, 4: 368–376

124   Liang Y, Wang H, Zhou J, *et al.* Covalent hybrid of spinel manganese-cobalt oxide and graphene as advanced oxygen reduction electrocatalysts. J Am Chem Soc, 2012, 134: 3517–3523

125   Zhang T, Cheng F, Du J, Hu Y, Chen J. Efficiently enhancing oxygen reduction electrocatalytic activity of MnO_2 using facile hydrogenation. Adv Energy Mater, doi: 10.1002/aenm.201400654

126   Du J, Zhang T, Cheng F, *et al.* Nonstoichiometric perovskite $CaMnO_{3-\delta}$ for oxygen electrocatalysis with high activity. Inorg Chem, 2014, 53: 9106–9114

127   Du J, Pan Y, Zhang T, *et al.* Facile solvothermal synthesis of $CaMn_2O_4$ nanorods for electrochemical oxygen reduction. J Mater Chem, 2012, 22: 15812–15818

128   Chen Y, Freunberger SA, Peng Z, Fontaine O, Bruce PG. Charging a Li–O_2 battery using a redox mediator. Nat Chem, 2013, 5: 489–494

129   Sun D, Shen Y, Zhang W, *et al.* A solution-phase bifunctional catalyst for lithium-oxygen batteries. J Am Chem Soc, 2014, 136: 8941–8946

130   Lim HD, Song H, Kim J, *et al.* Superior rechargeability and efficiency of lithium-oxygen batteries: hierarchical air electrode architecture combined with a soluble catalyst. Angew Chem, 2014, 126: 4007–4012

131   Yu M, Ren X, Ma L, Wu Y. Integrating a redox-coupled dye-sensitized photoelectrode into a lithium-oxygen battery for photoassisted charging. Nat Commun, 2014, 5: 5111

132   Hu X, Han X, Hu Y, Cheng F, Chen J. ε-MnO_2 nanostructures directly grown on Ni foam: a cathode catalyst for rechargeable Li-O_2 batteries. Nanoscale, 2014, 6: 3522–3525

133   Han X, Cheng F, Zhang T, *et al.* Hydrogenated uniform Pt clusters supported on porous $CaMnO_3$ as a bifunctional electrocatalyst for enhanced oxygen reduction and evolution. Adv Mater, 2014, 26: 2047–2051

134   Han X, Hu Y, Yang J, Cheng F, Chen J. Porous perovskite $CaMnO_3$ as an electrocatalyst for rechargeable Li-O_2 batteries. Chem Commun, 2014, 50: 1497–1499

135   Han X, Cheng F, Chen C, Hu Y, Chen J. Uniform MnO_2 nanostructures supported on hierarchically porous carbon as efficient electrocatalysts for rechargeable Li-O_2 batteries. Nano Res, doi: 10.1007/s12274-014-0604-y

136 Hu Y, Han X, Cheng F, *et al.* Size effect of lithium peroxide on charging performance of Li-O$_2$ batteries. Nanoscale, 2014, 6: 177–180

Kai Zhang was born in 1987. He received his BSc degree in materials chemistry from Nankai University (2010) and then joined the Key Laboratory of Advanced Energy Materials Chemistry (Ministry of Education) to study for his PhD degree. He is expecting to get his PhD in 2015 under the supervision of Professor Jun Chen. His research focuses on Li-ion batteries, Li-S batteries, and Na-ion batteries.

Jun Chen was born in 1967. He is a Cheung Kong Scholar Professor at the College of Chemistry, Nankai University, and Vice Chairman of the Chinese Society of Electrochemistry. He obtained his BSc and MSc degrees from Nankai University in 1989 and 1992, respectively, and his PhD from Wollongong University (Australia) in 1999. He held the NEDO fellowship at the National Institute of AIST Kansai Center (Japan) from 1999 to 2002. He has been working as the chair professor of energy chemistry at Nankai University since 2002. His research activity focuses on nanomaterials electrochemistry, batteries, fuel cells and solar cells.

中文摘要   作为电化学能源存储与转换的重要设备, 锂二次电池不断地改善着人类的生活. 为了满足人们对能量密度和功率密度不断增长的需求, 急需为锂离子电池和锂硫二次电池开发高容量、可快速充放的电极材料, 寻找用于可充式锂空气电池的高活性的催化剂. 高容量要求电极材料具有高的电荷转移数和小的分子质量, 快速的电荷转移要求材料离子传输距离短、反应活性位点多, 而设计制备纳米结构材料是改善电荷转移和离子电导率的有效手段. 本综述总结了最近在锂离子电池、锂硫二次电池和可充式锂空气电池中多电子反应的研究进展, 详细地讨论了提高电池倍率和循环性能的方法. 可发生多电子反应的先进的锂电池将成为未来的研究重点.